ARS ADVANCED ROBOTIC SYSTEMS INTERNATIONAL

Fuzzy/Kalman Hierarchical Horizontal Motion Control of Underactuated ROVs

Francesco M. Raimondi and Maurizio Melluso
Centro Interdipartimentale di Ricerca in Ingegneria dell'Automazione e dei Sistemi (CIRIAS), University of Palermo
Dipartimento di Ingegneria dell'Automazione e dei Sistemi, University of Palermo
Corresponding author E-mail: maurizio.melluso@alice.it

Abstract: *A new closed loop fuzzy motion control system including on-line Kalman's filter (KF) for the two dimensional motion of underactuated and underwater Remotely Operated Vehicle (ROV) is presented. Since the sway force is unactuated, new continuous and discrete time models are developed using a polar transformation. A new hierarchical control architecture is developed, where the high level fuzzy guidance controller generates the surge speed and the yaw rate needed to achieve the objective of planar motion, while the low level controller gives the thruster surge force and the yaw torque control signals. The Fuzzy controller ensures robustness with respect to uncertainties due to the marine environment, forward surge speed and saturation of the control signals. Also Lyapunov's stability of the motion errors is proved based on the properties of the fuzzy maps. If Inertial Measurement Unit data (IMU) is employed for the feedback directly, aleatory noises due to accelerometers and gyros damage the performances of the motion control. These noises denote a kind of non parametric uncertainty which perturbs the model of the ROV. Therefore a KF is inserted in the feedback of the control system to compensate for the above uncertainties and estimate the feedback signals with more precision.*
Keywords: *Fuzzy control , Kalman's filter, Lyapunov's stability, Motion control, ROV.*

1. Introduction

Underwater Robotic Vehicles (URV) are used in oceanographich studies and naval and archeological applications. The URV includes both Remotely Operated Vehicles (ROV) and Autonomous Underwater Vehicles (AUV). The ROV is normally used for the repairs of offshore structures or the inspection of the subsea environment (Antonelli et al., 2008, Koh et al., 2002). Actually URV operators are very sceptical about the prospect that AUVs will replace ROVs for inspection or repairs, so modern techniques are dedicated to designing advanced and intelligent ROVs with navigation systems (Ontini, 1998). In conventional operating, a human operator is in control and navigates the ROV by observing the images produced by an underwater camera. But a human in control is not efficient and not satisfactory because it is difficult to obtain a clear visual image from a camera and it is difficult to obtain a mathematical model of the environment around the ROV (Dai et al., 2002). Therefore, the priority of the ROV is to position itself, either tracking curves with autonomous navigation in the environment which has to be inspected, or near the structure of interest, against disturbances. Most ROVs are underactuated, so they have fewer control actuators than the number of independent directions of desired motion and in general, falls into category of so-called non-holonomic systems. However motion control strategies for non-holonomic Unmanned Aerial Vehicles (UAV) (Raimondi & Melluso, 2008) and for non-holonomic ground cars (Raimondi & Melluso, 2009) are not directly applicable to ROVs, because they are subjected to complex hydrodynamic factors (Fossen, 1994), they present unactuated dynamics and have a minimum surge control speed constraint that is greater than zero. Many ROVs operate in a crab-like manner with small roll and pitch angle that can be neglected during normal operations. Therefore it is useful to regard the vehicle's spatial motion as a superposition of two displacements: the motion in the vertical plane and the motion in the horizontal plane, so that it allows the ROV propulsion system to be divided into two independent subsystems responsible for movement in these planes respectively (Dobref & Tarabuta, 2007). For example the VideoRay ROV has two horizontal thrusters for planar motion and one for vertical motion (Miskovic et al., 2009). Motion control methodologies for ROVs have been put forward to handle external disturbances and parametric model uncertainties, i.e robust and adaptive control techniques, introducing the use of sliding-mode control (Yoerger & Slotine, 1985 ; Yoerger & Slotine, 1991). Hierarchical architecture for the motion control of underwater vehicles, which encompasses strategic, tactical and execution levels of control has been proposed (Valavanis et al., 1997). Horizontal motion control strategies have been developed adopting a dual-loop hierarchical guidance control scheme, based on a set of Lyapunov-based guidance task functions and a PI gain scheduling controller (Caccia & Verruggio, 2000). Vision-based conventional dual-loop hierarchical architecture for

International Journal of Advanced Robotic Systems, Vol. 7, No. 2 (2010)
ISSN 1729-8806, pp. 139-154

kinematic and kinetic control of the two dimensional motion of ROV has been developed (Caccia, 2007). Techniques of intelligent control have not been addressed in any of the above papers. The advantage of intelligent fuzzy systems is that the controller can be designed to apply heuristic rules that reflects the experiences of human experts and the membership functions are generally predefined according to the non-linearities of the system. A Fuzzy like proportional derivative (PD) controller for ROVs to control the yaw and the depth of the vehicle has been developed (Akkizidis et al., 2007). A Fuzzy logic system has been employed in ROV to perform autonomous navigation in 3D space (Day et al., 2002). Precise autonomous navigation remains a significant challenge for all underwater platforms (Hagen P.E. et al, 2009). One strategy is to employ the best possible inertial navigation system (INS) together with internal sensors, like for example accelerometers and gyros, as done by the Hugin navigation system (Jalving et al., 2003). However noise from the internal sensors of the INS is responsible for non-parametric uncertainties which perturb the localization of the ROV. Several alternatives have therefore been included for providing the integrated inertial navigation systems with position updates. Following the ROV with a survey vessel is the preferred method for obtaining maximum position accuracy (Hagen et al., 2009). The survey vessel is tethered to the ROV with an umbilical cable that relays control signals. It is powered down to the vehicle and returns sensor data, and it has to be equipped with a Global Position System (GPS) and Ultra Short Base Line (USLB) for tracking the ROV at all times. To obtain a good estimation of the vehicle's position, an off-line Kalman's Filter (KF) has been employed which processes data provided by exteroceptive (GPS and USLB) and internal sensors (Jwo et al., 2009 ; Fabrizi et al., 1998).

In this paper, to continue this line of research, a new closed loop fuzzy hierarchical horizontal motion control system with on-line KF for underactuated ROVs is presented. The following contributions are given:

1) New stochastical continuous time and sampled models for horizontal motion of underactuated ROVs. They are developed using polar coordinates to consider the unactuated sway direction. The continuous time model is necessary to apply the fuzzy guidance commands and the kinetic control laws, while the sampled model describes the transition relationship state during a sampling interval and it is necessary to apply the KF.

2) Hierarchical architecture which merges a new low level kinetic controller with a new high level Fuzzy inference system. The fuzzy controller is responsible for prescribing the ROV guidance laws in terms of the surge speed and yaw rate needed to achieve horizontal motion control objectives in the work space. The kinetic controller gives the surge force and the yaw torque and ensures the convergence of the actual speeds to the guidance commands. Suitably actuator allocation gives the actuator forces. Unlike previous works (Caccia, 2007; Day et al., 2002; Caccia & Verruggio, 2000), an intelligent fuzzy controller has been addressed with a dinamical approach, where asymptotical stability is built on Lyapunov's theory, based on the properties of the fuzzy control surfaces. In other words, the stability theorem provides conditions on the fuzzy control surfaces under which the motion errors are bounded and converge to zero. The fuzzy controller proposed in this paper ensures the robustness of the motion with respect to disturbances due to the marine environment, forward surge speed and saturation of the control signals.

3) A methodology for solving the on-line sensors data fusion using KF. Unlike to previous works (Jwo et al., 2009 ; Fabrizi et al., 1998), where off-line KF algorithms have been put forward to estimate the location of mobile vehicles, in this paper the KF is located in the feedback of the Fuzzy dynamic motion control system. It fuses data provided by internal and exteroceptive sensors, filters the noises of the internal sensors and obtains a good estimate of the feedback signals. In this way the KF compensates the effects of non-parametric uncertainties due to the noise of the internal sensors, i.e. discontinuities in the dynamics of the motion errors, guidance commands and force control signals.

This paper is organized as it follows. In Subsection 2.1 continuous time kinematic and dynamic models are presented for horizontal motion of an Underactuated ROV. The KF requires a stochastic sampled state space representation to be derived which is developed in subsection 2.2. Section 3.2 presents the new high level fuzzy control guidance commands, where the Lyapunov's theorem is used in order to investigate the asymptotical stability of the motion errors. Section 3.3 presents news kinetic control laws to obtain the surge force and the yaw torque from the guidance commands. Convergence of the actual speeds of the ROV to the fuzzy guidance commands is proved. In Section 3.4 the on-line KF algorithm is developed. Section 4 presents simulation experiments performed in a Matlab environment, where the effectiveness of our motion control system is shown.

2. Continuous and sampled time models for the two dimensional motion of ROV

This section focuses on the development of continuous and discrete time models for the planar motion of ROVs.

2.1. Continuous time dynamic model

Let (X, Y) be the Earth Fixed Reference System (ERF) and (x_b, y_b) be the fixed body frame (cf. Fig. 1). In normal operations the pitch and the roll angles are small, so they can be neglected. Therefore in the horizontal plane the following vectors may be considered:

$$\begin{aligned} \boldsymbol{\eta}(t) &= \left[x(t) \;\; y(t) \;\; \psi(t)\right]^{\mathbf{T}}, \\ \boldsymbol{\upsilon}(t) &= \left[u(t) \;\; v(t) \;\; r(t)\right]^{\mathbf{T}}, \end{aligned} \tag{1}$$

where:

$x(t)$, $y(t)$ represent the position coordinates with reference to the ERF;
$\psi(t)$ represent the yaw, i.e. the orientation of the ROV (Euler angle);
$u(t)$, $v(t)$ represent the surge and sway speeds respectively, i.e. the linear velocities along longitudinal and transversal axes evaluated in relation to the fixed body frame;
$r(t)$ represents the yaw rate, i.e. the angular velocity about the axis perpendicular to the plane (X,Y).
The velocity transformation in the horizontal plane assumes the following form:

$$\dot{\boldsymbol{\eta}}(t) = \mathbf{J}(\boldsymbol{\eta}(t))\boldsymbol{\upsilon}(t)\,, \tag{2}$$

where $\mathbf{J}(\boldsymbol{\eta})$ is the following matrix:

$$\mathbf{J}(\boldsymbol{\eta}(t)) = \begin{bmatrix} \cos(\psi(t)) & -\sin(\psi(t)) & 0 \\ \sin(\psi(t)) & \cos(\psi(t)) & 0 \\ 0 & 0 & 1 \end{bmatrix}. \tag{3}$$

In extensive form the result is:

$$\begin{aligned} \dot{x}(t) &= u(t)\cos\psi(t) - v(t)\sin\psi(t)\,, \\ \dot{y}(t) &= u(t)sen\psi(t) + v(t)\cos\psi(t)\,, \\ \dot{\psi}(t) &= r(t)\,. \end{aligned} \tag{4}$$

Practically all the trajectories are planned with combination of straightlines and arcs of circumference, so in many applications the reference surge velocity is positive and constant, while the reference yaw rate may be constant or null. However in (4) the presence of the sway speed is evident. It is responsible for translational motion with respect to the vehicle's longitudinal axis. In fact, the equations (4) require integration of the unactuated dynamics to obtain the planar trajectory from the surge and angular velocities. Therefore it is necessary to determine the dynamic model of the ROV. Indicate the thruster surge force with $\tau_u(t)$ and the yaw torque with $\tau_r(t)$.

Lemma 1. Assume the mass matrix of the ROV as the identity matrix. Then the dynamic model of the ROV assumes the following form:

$$\begin{aligned} \dot{u}(t) - v(t)r(t) &= \tau_u(t)\,, \\ \dot{v}(t) + r(t)u(t) &= 0\,, \\ \dot{r}(t) &= \tau_r(t)\,. \end{aligned} \tag{5}$$

Proof. The Lagrangian function of the system is given by:

$$L(\boldsymbol{\eta}(t), \dot{\boldsymbol{\eta}}(t)) = \frac{1}{2}\dot{x}^2(t) + \frac{1}{2}\dot{y}^2(t) + \frac{1}{2}\dot{\psi}^2(t)\,. \tag{6}$$

The equations of the planar motion can be obtained using the following Lagrange formulation:

$$\frac{d}{dt}\left(\frac{\partial L(\boldsymbol{\eta}(t), \dot{\boldsymbol{\eta}}(t))}{\partial \dot{\boldsymbol{\eta}}}\right) - \frac{\partial L(\boldsymbol{\eta}(t), \dot{\boldsymbol{\eta}}(t))}{\partial \boldsymbol{\eta}} = \boldsymbol{\tau}(t)\,, \tag{7}$$

where $\boldsymbol{\eta}(t)$ is given by (1), while $\boldsymbol{\tau}(t)$ is the following vector:

$$\boldsymbol{\tau}(t) = \begin{bmatrix} \tau_u(t)\cos\psi(t) & \tau_u(t)\sin\psi(t) & \tau_r(t) \end{bmatrix}^{\mathbf{T}}. \tag{8}$$

From the Lagrange equations (7) it follows that:

$$\begin{aligned} \ddot{x}(t) &= \tau_u(t)\cos\psi(t)\,, \\ \ddot{y}(t) &= \tau_u(t)sen\psi(t)\,, \\ \ddot{\psi}(t) &= \tau_r(t)\,. \end{aligned} \tag{9}$$

Differentiating equations (4) leads to the following model:

$$\begin{aligned} \ddot{x}(t) &= -r(t)u(t)\sin\psi(t) + \dot{u}(t)\cos\psi(t) + \\ &\quad -r(t)v(t)\cos\psi(t) - \dot{v}(t)\sin\psi(t), \\ \ddot{y}(t) &= r(t)u(t)\cos\psi(t) + \dot{u}(t)\sin\psi(t) + \\ &\quad -r(t)v(t)\sin\psi(t) + \dot{v}(t)\cos\psi(t), \\ \ddot{\psi}(t) &= \dot{r}(t). \end{aligned} \tag{10}$$

Multiplying the first and second equations of (10) by $\cos\psi(t)$ and $\sin\psi(t)$ respectively and adding the results, gives:

$$\dot{u}(t) = \ddot{x}(t)\cos\psi(t) + \ddot{y}(t)\sin\psi(t) + v(t)r(t). \tag{11}$$

From the dynamic equations (9) it follows that:

$$\ddot{x}(t)\cos\psi(t) + \ddot{y}(t)\sin\psi(t) = \tau_u(t). \tag{12}$$

Substituting equation (12) into (11), result is:

$$\dot{u}(t) = \tau_u(t) - v(t)r(t). \tag{13}$$

Multiplying the first and second equations of (10) by $\cos\psi(t)$ and subtracting these two equations leads to:

$$\ddot{x}(t)\sin\psi(t) - \ddot{y}(t)\cos\psi(t) = -r(t)u(t) - \dot{v}(t). \tag{14}$$

From the dynamic equations (9), the result is:

$$\ddot{y}(t)\cos\psi(t) - \ddot{x}(t)\sin\psi(t) = 0. \tag{15}$$

Substituting (15) into (14), it follows that:

$$\dot{v}(t) = -r(t)u(t). \tag{16}$$

Therefore the complete dynamic model is given by (5). Q.E.D.
Generally, the mass matrix of the ROV is not the identity matrix and the hydrodynamic added mass has to be considered. Indicate the mass of the ROV with m, the inertial moment about the axis perpendicular to the plane (x_b, y_b) with I_z and the hydrodynamic masses with $X_{\dot{u}}, Y_{\dot{v}}$ and $N_{\dot{r}}$. The dynamic model (5) may be rewritten as follows:

$$\begin{aligned} m_u\dot{u}(t) - m_v v(t)r(t) &= \tau_u(t)\,, \\ m_v\dot{v}(t) + m_u r(t)u(t) &= 0\,, \\ m_r\dot{r}(t) &= \tau_r(t)\,, \end{aligned} \tag{17}$$

where:

$$\begin{aligned} m_u &= m - X_{\dot{u}}\,, \\ m_v &= m - Y_{\dot{v}}\,, \\ m_r &= I_z - N_{\dot{r}}\,. \end{aligned} \tag{18}$$

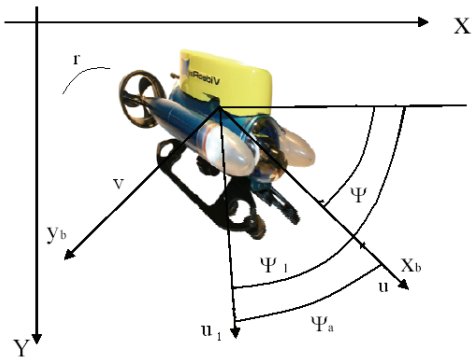

Fig. 1. ROV with reference systems.

Since the sway force is unavailable, the greatest difficulty for the control of the ROV is how to properly handle the vehicle's sway dynamics. To deal with this problem, the following polar coordinates transformation is defined (see Fig. 1):

$$\begin{aligned} u_l(t) &= \sqrt{u^2(t) + v^2(t)}\ , \\ \psi_l(t) &= \psi(t) + \psi_a(t)\ , \end{aligned} \tag{19}$$

where:

$$\psi_a(t) = \arctan[v(t)/u(t)] \tag{20}$$

is a polar angle and also called the sideslip angle [16]. Since the surge velocity is positive, it gives:

$$-0.5\pi \le \psi_a(t) \le 0.5\pi\ . \tag{21}$$

Differentiating the first equation of (19) and considering that:

$$\begin{aligned} u(t) &= u_l(t)\cos\psi_a(t), \\ v(t) &= u_l(t)\sin\psi_a(t), \end{aligned} \tag{22}$$

the ROV kinematic model (4) and the dynamic equations (17) may be rewritten as it follows:

$$\begin{aligned} &\dot{x}(t) = u_l(t)\cos\psi_l(t)\ , \\ &\dot{y}(t) = u_l(t)\sin\psi_l(t)\ , \\ &\dot{\psi}_l(t) = r(t) + \dot{\psi}_a(t) = r_l(t)\ , \\ &\tau_u(t) = m_u\dot{u}_l(t)/\cos\psi_a(t) - m_v v(t)r(t) + \\ &\qquad + \frac{m_u}{m_v} r(t)u(t)\tan\psi_a(t)\ , \\ &\tau_r(t) = m_r\dot{r}(t)\ . \end{aligned} \tag{23}$$

The accelerations of the ROV evaluated in relation to the ERF are given by:

$$\begin{bmatrix} \ddot{x}(t) \\ \ddot{y}(t) \\ \ddot{\theta}(t) \end{bmatrix} = \begin{bmatrix} u_l(t)\dot{\psi}_l(t) & \sin\psi_l(t) + \dot{u}_l(t)\cos\psi_l(t) \\ u_l(t)\dot{\psi}_l(t) & \cos\psi_l(t) + \dot{u}_l(t)\sin\psi_l(t) \\ & \dot{r}_l(t) \end{bmatrix}. \tag{24}$$

Formula (24) may be written in relation to the body reference system as follows:

$$\begin{bmatrix} \ddot{x}_B(t) \\ \ddot{y}_B(t) \end{bmatrix} = \begin{bmatrix} \cos(\psi_l(t) - \psi_a(t)) & \sin(\psi_l(t) - \psi_a(t)) \\ -\sin(\psi_l(t) - \psi_a(t)) & \cos(\psi_l(t) - \psi_a(t)) \end{bmatrix} \begin{bmatrix} \ddot{x}(t) \\ \ddot{y}(t) \end{bmatrix}. \tag{25}$$

Remark 1. The INS calculates the position velocity and acceleration of the ROV from an Inertial Measurement Unit (IMU). An IMU consists of accelerometers measuring specific force and gyros measuring angular rate. The output of the accelerometers gives data on the accelerations (24). Therefore the longitudinal and lateral positions may be evaluated by applying the inverse of (24) and then double integration, once the orientation of the ROV has been calculated from the data of the gyros.

Remark 2. Following the ROV with a survey vessel is the preferred method to obtain maximum position accuracy. The survey vessel is equipped with a Global Position System (GPS) and tracks the ROV with an Ultra Short Base Line (USLB). By combining GPS with USBL the position of the ROV may be estimated. The IMU typically employ data provided by GPS and USBL to correct errors in the IMU state estimate. The KF will combine data obtained from internal and external sensors to localize the ROV with more precision.

Indicate with $\mathbf{w}(t) \in R^3$ the following vector:

$$\mathbf{w}^{\mathrm{T}}(t) = \begin{bmatrix} w_1(t) & w_2(t) & w_3(t) \end{bmatrix} \tag{26}$$

where the components are the measurements of noise due to the IMU. Indicate the output vector of the external sensors constituted by GPS and USLB with $\boldsymbol{\xi}(t)$ and the noise vector with $\boldsymbol{\rho}(t) \in R^3$. The complete continuous time mathematical model for the two dimensional motion of the ROV with non-parametric uncertainties due to the noise of the sensors, is given by:

$$\begin{aligned} &\dot{x}_n(t) = u_l(t)\cos\psi_l(t) + w_1(t)\ , \\ &\dot{y}_n(t) = u_l(t)sen\psi_l(t) + w_2(t)\ , \\ &\dot{\psi}_{\ln}(t) = r(t) + \dot{\psi}_a(t) + w_3(t) = r_l(t) + w_3(t)\ , \\ &\boldsymbol{\xi}(t) = \begin{bmatrix} 1 & 0 & 0 \\ 0 & 1 & 0 \\ 0 & 0 & 1 \end{bmatrix} \begin{bmatrix} x(t) \\ y(t) \\ \psi_l(t) \end{bmatrix} + \boldsymbol{\rho}(t)\ , \\ &\tau_u(t) = m_u\dot{u}_l(t)/\cos\psi_a(t) - m_v v(t)r(t) + \\ &\qquad + \frac{m_u}{m_v} r(t)u(t)\tan\psi_a(t)\ , \\ &\tau_r(t) = m_r\dot{r}(t), \end{aligned} \tag{27}$$

where $x_n(t)$, $y_n(t)$ and $\psi_{\ln}(t)$ are the position and orientation of the ROV in presence of noise of the IMU.

2.2. Stochastical sampled odometric model

In this subsection a discrete time odometric model for planar motion of the ROV is set out. An analogical to digital converter obtains samples of $x(t), y(t)$ and $\psi_l(t)$. Assume a constant sampling period T and denote $k = kT$, $k \in Z$. Indicate the incremental distance traveled by the reference point (x, y) with $\Delta D(k)$ (cf. Fig. 2). It gives:

$$\begin{aligned} &\Delta D(k) = (\Delta d_{right}(k) + \Delta d_{left}(k))/2, \\ &k \in Z\ , \end{aligned} \tag{28}$$

where $\Delta d_{right}(k)$ and $\Delta d_{left}(k)$ are incremental distances traveled by the points in which the engines are located.

By considering the unactuated sway speed, the incremental distance traveled by the reference point is given by:

$$\Delta M(k) = \Delta D(k) / \cos(\psi_a(k)), \quad k \in Z. \tag{29}$$

Let parameter b be the distance between the right and the left thrusters. Assume the noises of the internal and external sensors given by $\mathbf{w}(k) \in R^3$ and $\boldsymbol{\rho}(k) \in R^3$ respectively to be random variables with Gaussian distributions, sequences that have zero cross-correlation with each other and zero mean (statistically), that is:

$$E[\mathbf{w}(k)] = \mathbf{0} \quad \text{and} \quad E[\boldsymbol{\rho}(k)] = \mathbf{0}\ ; \tag{30}$$

$$E\left[\mathbf{w}(i)\mathbf{w}^{\mathbf{T}}(j)\right] = \begin{cases} \mathbf{R}_{\mathbf{w}} & i = j \\ \mathbf{0} & i \neq j \end{cases}; \tag{31}$$

$$E\left[\boldsymbol{\rho}(i)\boldsymbol{\rho}^{\mathbf{T}}(j)\right] = \begin{cases} \mathbf{R}_{\boldsymbol{\rho}} & i = j \\ \mathbf{0} & i \neq j \end{cases}, \tag{32}$$

where $E[\cdot]$ represents expectation, $\mathbf{R}_{\mathbf{w}}$ is the process noise covariance matrix and $\mathbf{R}_{\boldsymbol{\rho}}$ is the measurement noise covariance matrix.
By assuming that:

$$\mu(k) = \psi_l(k) + (\Delta\psi_l(k) / 2)\ , \tag{33}$$

where

$$\Delta\psi_l(k) = (\Delta d_{right}(k) - \Delta d_{left}(k)) / b\cos(\psi_a(k)) \tag{34}$$

and after some algebra, the complete odometric model yields:

$$\begin{aligned} &\boldsymbol{\chi}(k+1) = \mathbf{A}(k)\boldsymbol{\chi}(k) + \mathbf{B}(k)\mathbf{u}(k) + \mathbf{w}(k)\ , \\ &\boldsymbol{\xi}(k) = \mathbf{C}(k)\boldsymbol{\chi}(k) + \boldsymbol{\rho}(k)\ , \end{aligned} \tag{35}$$

where:

$$\boldsymbol{\chi}^{\mathbf{T}}(k) = \left[x_n(k) \;\; y_n(k) \;\; \psi_{\ln}(k)\right],$$

$$\mathbf{A}(k) = \begin{bmatrix} 1 & 0 & -\Delta M(k)\sin(\mu(k)) \\ 0 & 1 & \Delta M(k)\cos(\mu(k)) \\ 0 & 0 & 1 \end{bmatrix},$$

$$\mathbf{B}(k) = \begin{bmatrix} \frac{1}{2}\cos(\mu(k)) + \frac{\Delta M(k)}{2b}\sin(\mu(k)) \ldots & \ldots \frac{1}{2}\cos(\mu(k)) - \frac{\Delta M(k)}{2b}\sin(\mu(k)) \\ \frac{1}{2}\sin(\mu(k)) - \frac{\Delta M(k)}{2b}\cos(\mu(k)) \ldots & \ldots \frac{1}{2}\sin(\mu(k)) + \frac{\Delta M(k)}{2b}\cos(\mu(k)) \\ -\frac{1}{b} & \frac{1}{b} \end{bmatrix}, \tag{36}$$

$$\mathbf{C}(k) = \begin{bmatrix} 1 & 0 & 0 \\ 0 & 1 & 0 \\ 0 & 0 & 1 \end{bmatrix},$$

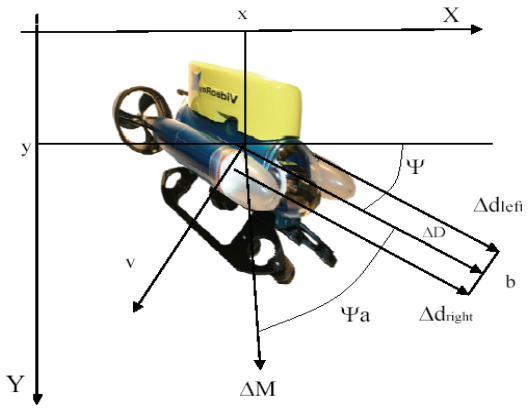

Fig. 2. ROV with odometric system

$$\mathbf{u}^{\mathbf{T}}(k) = \left[\ \Delta d_{left}(k) / \cos\psi_a(k) \quad \Delta d_{right}(k) / \cos\psi_a(k)\ \right],$$

$$\mathbf{w}^{\mathbf{T}}(k) = \left[\ w_1(k)\ w_2(k)\ w_3(k)\ \right],$$

$$\boldsymbol{\rho}^{\mathbf{T}}(k) = \left[\ \rho_1(k)\ \rho_2(k)\ \rho_3(k)\ \right].$$

3. Fuzzy hierarchical control system with on-line Kalman's filter for planar motion of underactuated ROVs

In this Section a new hierarchical control system for planar motion of underactuated ROVs is developed. A new high level fuzzy control obtains the guidance control laws, while a new low level controller generates the surge force command and the yaw torque control. A KF is inserted into the feedback of hierarchical control system to combine the data given by IMU, GPS and USLB and to obtain good estimates of the feedback position and orientation of the ROV. The fuzzy control system requires a knowledge of the model (23), while the KF requires a knowledge of the discrete time model (36).

3.1. Control problem formulation

Indicate the reference surge velocity and the reference yaw rate with $u_r(t)$ and $r_r(t)$ respectively. Also indicate the reference speeds in the presence of a certain sideslip angle with $u_{lr}(t)$ and $r_{lr}(t)$, and the time varying coordinates of the reference trajectory evaluated in relation to the ERF with $x_r(t), y_r(t)$ and $\psi_{lr}(t)$. The planar reference trajectory is given by the following equations:

$$\begin{aligned} &\dot{x}_r(t) = u_{lr}(t)\cos\psi_l(t)\ , \\ &\dot{y}_r(t) = u_{lr}(t)sen\psi_l(t)\ , \\ &\dot{\psi}_{lr}(t) = r_r(t) + \dot{\psi}_a(t) = r_{lr}(t)\ , \end{aligned} \tag{37}$$

where:

$$u_r(t) = u_{lr}(t)\cos\psi_a(t)\ . \tag{38}$$

Define the following vectors of the guidance laws:

$$\begin{aligned} &\boldsymbol{\alpha}_c^T(t) = \left[u_c(t) \quad r_c(t)\right]\ , \\ &0 < \rho_1 \le u_c(t) \le \rho_2, \\ &\rho_1, \rho_2 \in R^+ \end{aligned} \tag{39}$$

and:

$$\boldsymbol{\beta}_c(t)=\begin{bmatrix} u_c(t)/\cos\psi_a(t) \\ r_c(t)+\dot{\psi}_a(t) \end{bmatrix}=\begin{bmatrix} u_{lc}(t) \\ r_{lc}(t) \end{bmatrix}, \tag{40}$$

where $u_c(t)$ and $r_c(t)$ are the surge velocity and yaw rate controls respectively, while $u_{lc}(t)$ and $r_{lc}(t)$ are the guidance control laws in the presence of sideslip angle. The actual position and orientation of the ROV can be obtained as it follows:

$$\begin{aligned} &\dot{x}(t)=u_{lc}(t)\cos\psi_l(t), \\ &\dot{y}(t)=u_{lc}(t)sen\psi_l(t), \\ &\dot{\psi}_l(t)=r_c(t)+\dot{\psi}_a(t)=r_{lc}(t). \end{aligned} \tag{41}$$

Remark 3. The control velocity $u_{lc}(t)$ is positive every time, once the surge velocity control is positive.

Indicate the surge force and the yaw torque control signals respectively with $\tau_{uc}(t)$ and $\tau_{rc}(t)$ and with $\boldsymbol{\alpha}(t)$ the following vector:

$$\boldsymbol{\alpha}^{\mathrm{T}}(t)=\begin{bmatrix} u(t) & r(t) \end{bmatrix}, \tag{42}$$

where $u(t)$ and $r(t)$ denote the actual surge speed and yaw rate, i.e. the virtual controls. Let $u_l(t)$ and $r_l(t)$ be the same functions in the presence of sway.

The control system put forward in this paper is made up of two hierarchical levels. The high level controller gives the guidance commands (40), so that the following tracking errors evaluated in relation to the ROV body frame:

$$\mathbf{e}(t)=\begin{bmatrix} e_x(t) \\ e_y(t) \\ e_{\psi l}(t) \end{bmatrix}=\begin{bmatrix} \cos\psi_l(t) & \sin\psi_l(t) & 0 \\ -\sin\psi_l(t) & \cos\psi_l(t) & 0 \\ 0 & 0 & 1 \end{bmatrix}\begin{bmatrix} x_r(t)-x(t) \\ y_r(t)-y(t) \\ \psi_{l\,r}(t)-\psi_l(t) \end{bmatrix} \tag{43}$$

are bounded and converge to zero. A new Fuzzy controller will be employed without reference to the forces and moments that generates such motion. However, the dynamics of the ROV are given by the fourth and fifth equations in (27); therefore, the low level controller gives the functions $\tau_{uc}(t)$ and $\tau_{rc}(t)$ to ensure convergence to zero of the following error:

$$\begin{aligned} \bar{\mathbf{e}}(t)=\boldsymbol{\alpha}_{\mathbf{c}}(t)-\boldsymbol{\alpha}(t)=\begin{bmatrix} e_u(t) \\ e_r(t) \end{bmatrix}=\begin{bmatrix} u_c(t)-u(t) \\ r_c(t)-r(t) \end{bmatrix}= \\ =\begin{bmatrix} (u_{lc}(t)-u_l(t))\cos\psi_a(t) \\ (r_{lc}(t)-r_l(t)) \end{bmatrix}. \end{aligned} \tag{44}$$

If the virtual controls converge to the guidance control laws, then the high level control ensures the trajectory tracking. When the velocities $u_l(t)$ and $r_l(t)$ are applied to the ROV, the IMU evaluates the position and orientation of the submarine vehicle through the integration of the following equations (see. Eqs. 27):

$$\begin{aligned} &\dot{x}_n(t)=u_l(t)\cos\psi_l(t)+w_1(t), \\ &\dot{y}_n(t)=u_l(t)sen\psi_l(t)+w_2(t), \\ &\dot{\psi}_{\ln}(t)=r(t)+\dot{\psi}_a(t)+w_3(t)=r_l(t)+w_3(t). \end{aligned} \tag{45}$$

Aleatory noises of the IMU made by the components of the vector (26) cause non-parametric uncertainties which perturb the model and, therefore, the measurements of the ROV's position. They can corrupt the performance of the control system in terms of the dynamics of the motion errors given by (43). Measurements obtained by GPS and USLB are necessary to correct the localization of the ROV. The KF will estimate the filtered state from the outputs of the IMU and the outputs of the exteroceptive sensors, i.e. it will estimate the actual feedback position and orientation of the ROV. The filter above requires the linear discrete time stochastic state space representation given by (35) to be obtained. Then, an estimation of the feedback signals, using a 'Digital to Analogic Converter' (DAC) with 'Zero Order Hold' (ZOH) provides analogical information for generating the motion errors (43) and for applying the high level guidance control laws (40) and the low level control signals.

3.2. High level Fuzzy guidance laws

The problem is to determine the guidance laws given by (39) and (40), where $u_{lc}(t)$ has to be saturated and must be a forward velocity, so that the Lyapunov's asymptotical stability of the tracking errors given by (43) is ensured. The following fuzzy guidance control laws are proposed:

$$\begin{aligned} &u_c(t)=f(\mathbf{e}(t))*\cos\psi_a(t)+u_r(t), \\ &r_c(t)=[r_r(t)+\dot{\psi}_a(t)]+[u_r(t)/\cos\psi_a(t)]\times \\ &\qquad\times[g(\mathbf{e}(t))+h(\mathbf{e}(t))\sin e_{\psi l}(t)], \\ &u_{c\max}\geq u_c(t)\geq 0, \\ &u_r(t)>0 \quad \forall t, \end{aligned} \tag{46}$$

where the nonlinear functions $f(\mathbf{e}(t))$, $g(\mathbf{e}(t))$ and $h(\mathbf{e}(t))$ are continuous and differentiable. The functions (40) are as follows:

$$\begin{aligned} &u_{lc}(t)=f(\mathbf{e}(t))+u_{lr}(t), \\ &r_{lc}(t)=r_{lr}(t)+u_{lr}(t)[g(\mathbf{e}(t))+h(\mathbf{e}(t))\sin e_{\psi l}(t)], \\ &u_{lc\max}\geq u_{lc}(t)\geq 0, \\ &u_{lr}(t)>0 \quad \forall t. \end{aligned} \tag{47}$$

The functions $f(\mathbf{e}(t)), g(\mathbf{e}(t))$ and $h(\mathbf{e}(t))$ are the crisp outputs of a fuzzy controller. The Fuzzy inference system is now described. The following linguistic labels are defined:

S=Small;
M=Medium;
H=High;
Opp=Opposite.

The input and output Fuzzy memberships are generalized bell functions and they are shown in Figs. 3 and 4. The fuzzy rules are shown in Table 1. The fuzzy controller is shown in Fig. 5. Fig. 6-8 show the fuzzy control surfaces.

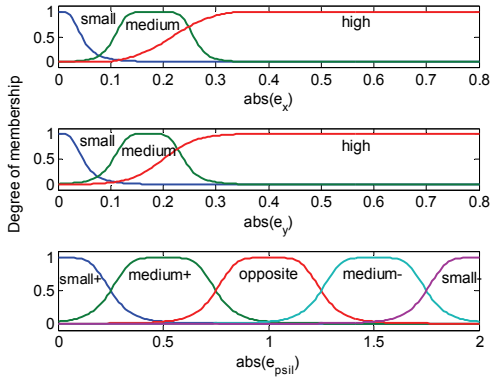

Fig. 3. Input fuzzy membership functions

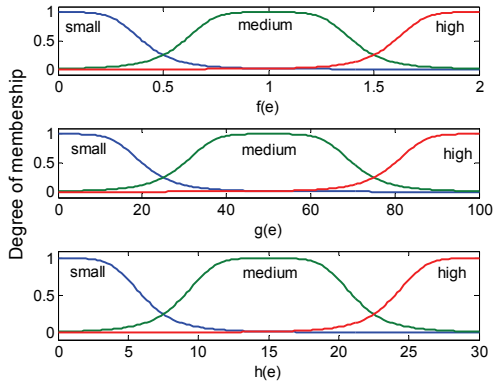

Fig. 4. Output fuzzy membership functions

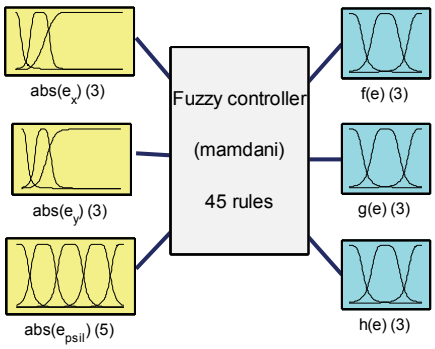

Fig. 5. Fuzzy controller

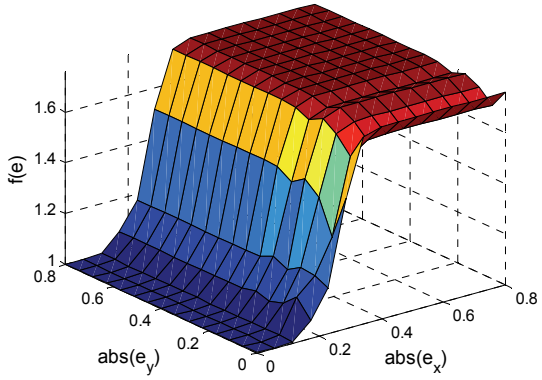

Fig. 6. Fuzzy control surface with constant lateral error

TABLE I Fuzzy Rules

If abs(e_x) is S and abs(e_y) is S and abs($e_{\psi l}$) is S+ then *f(e)* is S and *g(e)* is S and *h(e)* is S
If abs(e_x) is S and abs(e_y) is M and abs($e_{\psi l}$) is S+ then *f(e)* is S and *g(e)* is M and *h(e)* is S
If abs(e_x) is S and abs(e_y) is H and abs($e_{\psi l}$) is S+ then f(*e*) is M and *g(e)* is H and *h(e)* is S
If abs(e_x) is M and abs(e_y) is S and abs($e_{\psi l}$) is S+ then *f(e)* is M and *g(e)* is S and *h(e)* is S
If abs(e_x) is M and abs(e_y) is M and abs($e_{\psi l}$) is S+ then *f(e)* is M and *g(e)* is M and *h(e)* is S
If abs(e_x) is M and abs(e_y) is H and abs($e_{\psi l}$)is S+ then *f(e)* is M and *g(e)* is H and *h(e)* isS
If abs(e_x) is H and abs(e_y) is S and abs($e_{\psi l}$) is S+ then *f(e)* is H and *g(e)* is M and *h(e)* is S
If abs(e_x) is H and abs(e_y) is M and abs($e_{\psi l}$) is S+ then *f(e)* is H and *g(e)* is M and *h(e)* is S
If abs(e_x) is H and abs(e_y) is H and abs($e_{\psi l}$) is S+ then *f(e)* is H and *g(e)* is H and *h(e)* is S
If abs(e_x) is S and abs(e_y) is S and abs($e_{\psi l}$) is M+ then *f(e)* is M and *g(e)* is M and *h(e)* is M
If abs(e_x) is S and abs(e_y) is M and abs($e_{\psi l}$) is M+ then *f(e)* is M and *g(e)* is M and *h(e)* is M
If abs(e_x) is S and abs(e_y) is H and abs($e_{\psi l}$) is M+ then *f(e)* is M and *g(e)* is H and *h(e)* is M
If abs(e_x) is M and abs(e_y) is S and abs($e_{\psi l}$) is M+ then *f(e)* is M and *g(e)* is M and *h(e)* is M
If abs(e_x) is M and abs(e_y)is H and abs($e_{\psi l}$) is M+ then *f(e)* is M and*g(e)* is H and *h(e)* is M
If abs(e_x) is H and abs(e_y) is S and abs($e_{\psi l}$) is M+ then *f(e)* is H and *g(e)* is M and *h(e)* is M
If abs(e_x) is H and abs(e_y) is M and abs($e_{\psi l}$) is M+ then *f(e)* is H and *g(e)* is M and *h(e)* is M
If abs(e_x) is H and abs(e_y) is H and abs($e_{\psi l}$) is M+ then *f(e)* is H and *g(e)* is H and *h(e)* is M
If abs(e_x) is S and abs(e_y) is S and abs($e_{\psi l}$) is OPP then *f(e)* is M and *g(e)* is M and *h(e)* is H
If abs(e_x) is S and abs(e_y) is M and abs($e_{\psi l}$) is OPP then *f(e)* is M and*g(e)* is M and *h(e)* is H
If abs(e_x) is S and abs(e_y) is H and abs($e_{\psi l}$) is OPP then *f(e)* is M and*g(e)* is H and *h(e)* is H
If abs(e_x) is M and abs(e_y) is S and abs($e_{\psi l}$) is OPP then *f(e)* is M and*g(e)* is M and *h(e)* is H
If abs(e_x)is M and abs(e_y) is M and abs($e_{\psi l}$)is OPP then *f(e)* is M and*g(e)* is M and *h(e)*is H
If abs(e_x)is M and abs(e_y) is H and abs($e_{\psi l}$)is OPP then *f(e)* is M and*g(e)* is H and *h(e)*is M
If abs(e_x) is H and abs(e_y) is S and abs($e_{\psi l}$) is OPP

then $f(\boldsymbol{e})$ is H and $g(\boldsymbol{e})$ is M and h(**e**) is H
If abs(e_x) is H and abs(e_y)is M and abs($e_{\psi\, l}$)is OPP
then $f(\boldsymbol{e})$ is H and $g(\boldsymbol{e})$ is M and $h(\boldsymbol{e})$ is H
If abs(e_x)is H and abs(e_y) is H and abs($e_{\psi\, l}$) is OPP
then $f(\boldsymbol{e})$ is H and $g(\boldsymbol{e})$ is H and $h(\boldsymbol{e})$ is H
If abs(e_x) is S and abs(e_y) is S and abs($e_{\psi\, l}$) is M-
then $f(\boldsymbol{e})$ is M and $g(\boldsymbol{e})$ is M and $h(\boldsymbol{e})$ is M
If abs(e_x)is S and abs (e_y)is M and abs ($e_{\psi\, l}$)is M- then
$f(\boldsymbol{e})$ is M and $g(\boldsymbol{e})$ is M and $h(\boldsymbol{e})$ is M
If abs (e_x) is S and abs (e_y)is H and abs ($e_{\psi\, l}$) is M-
then $f(\boldsymbol{e})$ is M and $g(\boldsymbol{e})$ is H and $h(\boldsymbol{e})$ is M
If abs (e_x) is M and abs (e_y) is S and abs ($e_{\psi\, l}$)is M-
then $f(\boldsymbol{e})$ is M and $g(\boldsymbol{e})$ is M and $h(\boldsymbol{e})$ is M
If abs (e_x) is M and abs (e_y) is M and abs($e_{\psi\, l}$)is M-
then $f(\boldsymbol{e})$ is M and $g(\boldsymbol{e})$ is M and $h(\boldsymbol{e})$ is M
If abs (e_x) is M and abs (e_y) is H and abs($e_{\psi\, l}$)is M-
then $f(\boldsymbol{e})$ is M and $g(\boldsymbol{e})$ is H and $h(\boldsymbol{e})$ is M
If abs (e_x)is H and abs (e_y) is S and abs ($e_{\psi\, l}$)is M-
then $f(\boldsymbol{e})$ is H and $g(\boldsymbol{e})$ is M and $h(\boldsymbol{e})$ is M
If abs (e_x) is H and abs (e_y) is M and abs($e_{\psi\, l}$)is M-
then $f(\boldsymbol{e})$ is H and $g(\boldsymbol{e})$ is M and $h(\boldsymbol{e})$ is M
If abs (e_x) is H and abs (e_y) is H and abs ($e_{\psi\, l}$)is M-
then $f(\boldsymbol{e})$ is H and $g(\boldsymbol{e})$ is H and $h(\boldsymbol{e})$ is M
If abs (e_x) is S and abs (e_y) is S and abs ($e_{\psi\, l}$) is S-
then $f(\boldsymbol{e})$ is S and $g(\boldsymbol{e})$ is S and $h(\boldsymbol{e})$ is S
If abs (e_x) is S and abs(e_y) is M and abs ($e_{\psi\, l}$) is S-
then $f(\boldsymbol{e})$ is S and $g(\boldsymbol{e})$ is M and $h(\boldsymbol{e})$ is S
If abs (e_x) is S and abs (e_y) is H and abs ($e_{\psi\, l}$) is S-
then $f(\boldsymbol{e})$ is M and $g(\boldsymbol{e})$ is H and $h(\boldsymbol{e})$ is S
If abs (e_x) is M and abs (e_y) is S and abs ($e_{\psi\, l}$) is S-
then $f(\boldsymbol{e})$ is M and $g(\boldsymbol{e})$ is S and $h(\boldsymbol{e})$ is S
If abs (e_x) is M and abs (e_y) is M and abs ($e_{\psi\, l}$)is S-
then $f(\boldsymbol{e})$ is M and $g(\boldsymbol{e})$ is M and $h(\boldsymbol{e})$ is S
If abs (e_x) is M and abs (e_y) is H and abs ($e_{\psi\, l}$) is S-
then $f(\boldsymbol{e})$ is M and $g(\boldsymbol{e})$ is H and $h(\boldsymbol{e})$ is S
If abs (e_x)is H and abs (e_y) is S and abs ($e_{\psi\, l}$) is S-
then $f(\boldsymbol{e})$ is H and $g(\boldsymbol{e})$ is M and $h(\boldsymbol{e})$ is S
If abs (e_x) is H and abs(e_y) is M and abs ($e_{\psi\, l}$)is S-
then $f(\boldsymbol{e})$ is H and $g(\boldsymbol{e})$ is M and $h(\boldsymbol{e})$ is S
If abs(e_x) is H and abs (e_y) is H and abs($e_{\psi\, l}$) is S-
then $f(\boldsymbol{e})$ is H and $g(\boldsymbol{e})$ is H and $h(\boldsymbol{e})$ is S

Fig. 5 and Table 1 show that the inputs of the fuzzification process are the absolute values of the tracking errors given by (42). The implemented method for the logical 'and' and for the implication are the 'minimum' and the 'fuzzy minimum'. The consequents of each rule have been recombined using a maximum method. The defuzzyfication method is the 'centroid'. The input ranges are [0m-0.8m] for the position errors

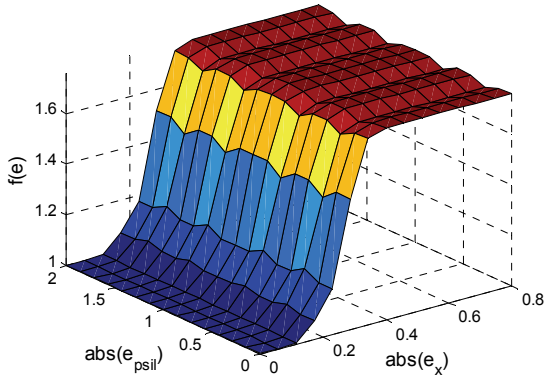

Fig. 7. Fuzzy control surface with constant orientation error

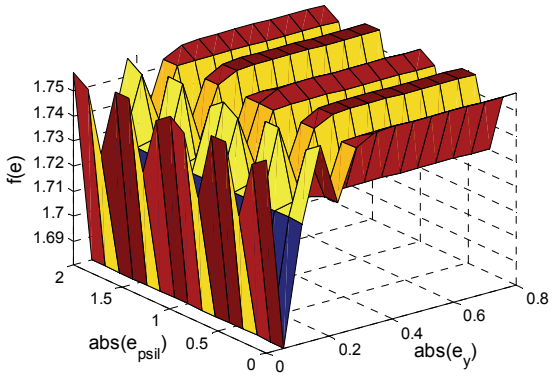

Fig. 8. Fuzzy control surface with constant longitudinal error

and [0rad- 2rad] for the orientation error. The outputs of the fuzzy system are crisp values that are the numerical values of the functions $f(\mathbf{e}(t)), g(\mathbf{e}(t))$ and $h(\mathbf{e}(t))$. The input and output ranges may be subjected to changes manually to optimiz the convergence of the tracking errors and the robustness in relation to possible disturbances due to the marine environment.

To ensure the Lyapunov's stability of the motion errors given by (43), analytical properties of the fuzzy maps must be satisfied.

Assumption 1. The membership functions have to be chosen in order to satisfy the following properties of the fuzzy control surfaces:

$$\textit{Property 1:}\quad \begin{aligned} f(\mathbf{e}(t)) = 0 &\Leftrightarrow \mathbf{e}(t) = \mathbf{0}\,, \\ g(\mathbf{e}(t)) = 0 &\Leftrightarrow \mathbf{e}(t) = \mathbf{0}\,, \\ h(\mathbf{e}(t)) = 0 &\Leftrightarrow \mathbf{e}(t) = \mathbf{0}\,. \end{aligned} \tag{48}$$

$$\textit{Property 2:}\quad 0 \le f(\mathbf{e}(t)) \le f_{\max}\,. \tag{49}$$

$$\textit{Property 3:}\quad 0 \le g(\mathbf{e}(t)) \le g_{\max}\,. \tag{50}$$

$$\textit{Property 4:}\quad 0 \le h(\mathbf{e}(t)) \le h_{\max}\,. \tag{51}$$

$$\textit{Property 5:}\quad \sum_{j=0}^{M-1}\left[\int_{j}^{j+1} g(\mathbf{e}(t))dt\right] > 0, j \in N, M > 0\,. \tag{52}$$

$$\textit{Property 6:}\quad \begin{aligned} &\frac{\partial f(\mathbf{e}(t))}{\partial e_x} > 0; \frac{\partial f(\mathbf{e}(t))}{\partial e_y} \cong 0; \frac{\partial f(\mathbf{e}(t))}{\partial e_{\psi l}} \cong 0, \\ &\frac{\partial g(\mathbf{e}(t))}{\partial e_x} \cong 0; \frac{\partial g(\mathbf{e}(t))}{\partial e_y} > 0; \frac{\partial g(\mathbf{e}(t))}{\partial e_{\psi l}} \cong 0, \\ &\frac{\partial h(\mathbf{e}(t))}{\partial e_x} \cong 0; \frac{\partial h(\mathbf{e}(t))}{\partial e_y} \cong 0; \frac{\partial h(\mathbf{e}(t))}{\partial e_{\psi\, l}} > 0. \end{aligned} \quad (53)$$

Remark 4. The fuzzy control surfaces shown in Figs. 6-8 ensure the satisfaction of the properties given by (48)-(53).
Remark 5. From Fig. 8 it is evident that the function $f(\mathbf{e}(t))$ does not change significantly when the lateral and orientation change. The symmetries of the functions $g(\mathbf{e}(t))$ and $h(\mathbf{e}(t))$ are the same as the function $f(\mathbf{e}(t))$.
Remark 6. The property given by (49) ensures that:

$$u_{lr}(t) = \rho_1 \le u_{lc}(t) \le \rho_2 = f_{\max} + u_{lr}(t) \ , \quad (54)$$

where $f_{\max}$ is the maximum of the function $f(\mathbf{e}(t))$. Note that the saturation value of the surge speed depends on the numerical value of $f_{\max}$.
Remark 7. The following conditions have been satisfied:

$$\begin{aligned} &u_{lr}(t) > 0 \ \ \forall t, \\ &f(\mathbf{e}) \in [0 \ \ f_{\max}], \\ &f_{\max} > 0 \ . \end{aligned} \quad (55)$$

Therefore the surge control speed of the ROV may be bounded because it has forward command and the maximum values may be regulated by varying the maximum value of the function $f(\mathbf{e}(t))$.
Taking into account the derivative of the errors (43), by suitably replacing (41) and (47) with it, the following closed loop mathematical model is obtained:

$$\dot{\mathbf{e}}(t) = \begin{bmatrix} (r_{l\,r}(t) + u_{l\,r}(t) g(\mathbf{e}(t)) + h(\mathbf{e}(t)) \sin e_{\psi l}(t)) e_y(t) + \\ +(f(\mathbf{e}(t)) + u_{l\,r}(t)(1 - \cos e_{\psi l}(t))) \\ -(r_{l\,r}(t) + u_{l\,r}(t)(g(\mathbf{e}(t)) + h(\mathbf{e}(t)) \sin e_{\psi l}(t)) e_x + \\ +u_{l\,r}(t)\sqrt{1 - \cos^2 e_{\psi l}(t)} \\ -u_{l\,r}(t)(g(\mathbf{e}(t)) + h(\mathbf{e}(t)) \sin e_{\psi l}(t)) \end{bmatrix} . \quad (56)$$

Now a reformulation of the theorem presented in Raimondi & Melluso, 2008, is given for the underactuated ROV.
Theorem 1. Consider the mathematical model of the ROV given by (41), in closed loop with the fuzzy control law given by (47). Under assumption 1, the equilibrium state of the closed loop fuzzy navigation system given by (56) is the origin of the state space and it is asymptotically stable.
Proof. If the properties given by (48) are satisfied, then the equilibrium state of the representation (56) is the origin of the state space. We chooose the following Lyapunov's function:

$$\begin{aligned} V_0 = &(f(\mathbf{e}(t)) + g(\mathbf{e}(t))) + (1 - \cos e_{\psi\, l}(t)) \times \\ &\times \sum_{j=0}^{M-1} \left(\int_j^{j+1} g(\mathbf{e}(t)) dt \right) . \end{aligned} \quad (57)$$

Differentiating the function (57) and considering the analytical properties given by (53) lead to:

$$\begin{aligned} \dot{V}_0 = &\frac{\partial f(\mathbf{e}(t))}{\partial e_x} (f(\mathbf{e}(t) + u_r(t)(1 - \cos\ e_{\psi\, l})) + \\ &+ u_r(t)\sqrt{1 - \cos^2 e_{\psi\, l}(t)} \frac{\partial g(\mathbf{e}(t))}{\partial e_y} \ ) + \\ &+ \left[\sqrt{1 - \cos^2 e_{\psi\, l}(t)} u_r(t) g(\mathbf{e}(t)) \sum_{j=0}^{M-1} \left(\int_j^{j+1} g(\mathbf{e}(t)) dt \ \right) \right] + \\ &- \left[u_r(t) h(\mathbf{e}(t)) \sin^2 e_{\psi\, l}(t) \sum_{j=0}^{M-1} \left(\int_j^{j+1} g(\mathbf{e}(t)) dt \ \right) \right] + \\ &+ \left[(1 - \cos\ e_{\psi\, l}(t)) \sum_{j=0}^{M-1} g(\mathbf{e}(j)) \right] . \end{aligned} \quad (58)$$

Based on the properties (48)-(52), the function (57) is definite positive. Assuming the reference longitudinal $u_{lr}(t)$ positive every time leads to the following mathematical relations:

$$\begin{aligned} &0 \le \sqrt{1 - \cos^2 e_{\psi\, 1}(t)} u_r(t) \frac{\partial g(\mathbf{e}(t))}{\partial e_y} \Bigg) < \\ &< \sqrt{1 - \cos^2 e_{\psi\, 1}(t)} u_r(t) g(\mathbf{e}(t)) \sum_{j=0}^{M-1} \left(\int_j^{j+1} g(\mathbf{e}(t)) dt \ \right) \\ &u_r(t) h(\mathbf{e}(t)) (1 - \cos^2 e_{\psi\, 1}(t)) \sum_{j=0}^{M-1} \left(\int_j^{j+1} g(\mathbf{e}(t)) dt \ \right) > \\ &> (1 - \cos e_{\psi\, 1}(t)) \sum_{j=0}^{M-1} g(\mathbf{e}(j)) \ge 0 \ . \end{aligned} \quad (59)$$

Consequently, function (58) is definite negative. Therefore the equilibrium point of the closed loop system (56) is asymptotically stable. Q.E.D.

3.3. Low level kinetic controller

In this subsection news thruster surge force and yaw torque control laws are proposed for the underactuated system given by (23). The dynamic effects lead to the error given by (44), where $u_{lc}(t)$ and $r_{lc}(t)$ are the fuzzy guidance control laws given by (47), $u_l(t)$ and $r_l(t)$ are the actual velocities of the ROV, while $\psi_a(t)$ is the sideslip angle given by (20). From the fourth and fifth equations of (23), the surge force and the yaw torque are obtained as follows:

$$\begin{aligned} &\tau_u(t) = m_u \dot{u}_l(t) / \cos\psi_a(t) - m_v v(t) r(t) + \frac{m_u}{m_v} r(t) u(t) \tan\psi_a(t) \ , \\ &\tau_r(t) = \dot{r}(t) \ . \end{aligned} \quad (60)$$

The problem is to determine a surge force control and a yaw torque control, which ensure the convergence to zero of the error given by (44). The following dynamical control laws are proposed:

$$\begin{aligned}
&\tau_{rc}(t) = m_r[\dot{r}_{lc}(t) - \ddot{\psi}_a(t)] + \bar{K} m_r[r_{lc}(t) - \dot{\psi}_a(t) - r(t)] \,, \\
&\tau_{uc}(t) = \frac{m_u \dot{u}_{lc}(t)}{\cos\psi_a(t)} + m_u[r_{lc}(t) - \dot{\psi}_a(t)] \times \\
&\quad \times \int_0^t [r_{lc}(t) - \dot{\psi}_a(t)] u_{lc}(t) \cos\psi_a(t) dt + \\
&\quad + \frac{m_u}{m_v} \left[\; (r_l(t) - \dot{\psi}_a(t)) u_l(t) \sin\psi_a(t) \; \right] + \\
&\quad + \frac{K m_u}{\cos\psi_a(t)} (u_{lc}(t) - u_l(t)) \,, \\
&\bar{K}, K \in R^+ .
\end{aligned} \tag{61}$$

Now the following theorem can be formulated.

Theorem 2. Consider the ROV system given by (23) in closed loop with the fuzzy guidance laws (47) and with the kinetic control laws (61). Then the speeds error given by (44) converge asymptotically to zero.

Proof. From the second equation of (60) and first equation of (50) it follows that:

$$m_r[\dot{r}_{lc}(t) - \ddot{\psi}_a(t) - \dot{r}(t)] + \bar{K} m_r[r_{lc}(t) - \dot{\psi}_a(t) - r(t)] = 0. \tag{62}$$

By using $\varepsilon(t)$ to indicate the following error:

$$\varepsilon(t) = r_{lc}(t) - \dot{\psi}_a(t) - r(t) \,, \tag{63}$$

the differential equation (62) can be rewritten as it follows:

$$\dot{\varepsilon}(t) + \bar{K}\varepsilon(t) = 0 \,. \tag{64}$$

It appears that, if the value of $\bar{K}$ is sufficiently large, then the function $\varepsilon(t)$ converge to zero rapidly. It gives:

$$\lim_{t\to\infty}[r_{lc}(t) - \dot{\psi}_a(t) - r(t)] = 0 \,. \tag{65}$$

It implies that:

$$\lim_{t\to\infty}[r_c(t) - r(t)] = 0 \,, \tag{66}$$

so the second component of the vector (44) converges asymptotically to zero. Now, by considering that:

$$v(t) = -\frac{m_u}{m_v}\int_0^t r(t)u(t)dt = -\frac{m_u}{m_v}\int_0^t r(t)u_l(t)\cos\psi_a(t)dt \,, \tag{67}$$

replacing (67) in the first equation of (60), the surge force given by the third equation of (23) is calculated by:

$$\begin{aligned}
\tau_u(t) &= m_u \dot{u}_l(t) / \cos\psi_a(t) \; + m_u[r_l(t) - \dot{\psi}_a(t)] \times \\
&\times \; \int_0^t [r_l(t) - \dot{\psi}_a(t)] u_l(t) \cos\psi_a(t) dt + \\
&+ \; \frac{m_u}{m_v} \; [r_l(t) - \dot{\psi}_a(t)] u_l(t) \sin\psi_a(t) \,.
\end{aligned} \tag{68}$$

By choosing the surge torque control that results from the second equation of (61), gives:

$$\begin{aligned}
&m_u \dot{u}_l(t) / \cos\psi_a(t) \; + m_u[r_l(t) - \dot{\psi}_a(t)] \times \\
&\times \; \int_0^t [r_l(t) - \dot{\psi}_a(t)] u_l(t) \cos\psi_a(t) dt + \frac{m_u}{m_v} \; [r_l(t) - \dot{\psi}_a(t)] \times \\
&\times u_l(t) \sin\psi_a(t) = \frac{m_u \dot{u}_{lc}(t)}{\cos\psi_a(t)} + m_u[r_{lc}(t) - \dot{\psi}_a(t)] \times \\
&\times \int_0^t [r_{lc}(t) - \dot{\psi}_a(t)] u_{lc}(t) \cos\psi_a(t) dt + \\
&+ \frac{m_u}{m_v} \; [r_l(t) - \dot{\psi}_a(t)] u_l(t) \sin\psi_a(t) + \frac{K m_u}{\cos\psi_a(t)} [u_{lc}(t) - u_l(t)] \,.
\end{aligned} \tag{69}$$

It follows:

$$\begin{aligned}
&\frac{m_u(\dot{u}_{lc}(t) - \dot{u}_l(t))}{\cos\psi_a(t)} \; + \frac{K m_u}{\cos\psi_a(t)} [u_{lc}(t) - u_l(t)] + \\
&m_u[r_{lc}(t) - \dot{\psi}_a(t)] \int_0^t [r_{lc}(t) - \dot{\psi}_a(t)] \; u_{lc}(t) \cos\psi_a(t) dt + \\
&- m_u[r_l(t) - \dot{\psi}_a(t)] \; \int_0^t [r_l(t) - \dot{\psi}_a(t)] \; u_l(t) \cos\psi_a(t) dt = 0 \,.
\end{aligned} \tag{70}$$

Since the virtual orientation control converges to the fuzzy guidance law (cf. eq. 65), equation (70) in a steady state may be formulated in the following way:

$$\begin{aligned}
&m_u[\dot{u}_{lc}(t) - \dot{u}_l(t)] \cos\psi_a(t) \; + K m_u \cos\psi_a(t)[u_{lc}(t) - u_l(t)] + \\
&+ m_u r(t) \cos^2\psi_a(t) \int_0^t \; r(t)[u_{lc}(t) - u_l(t)] \cos\psi_a(t) dt = 0 \,.
\end{aligned} \tag{71}$$

From the first equation of (22) it follows that:

$$\begin{aligned}
&m_u[\dot{u}_c(t) - \dot{u}(t)] \; + K m_u[u_c(t) - u(t)] + \\
&+ m_u r(t) \cos^2\psi_a(t) \int_0^t \; r(t)[u_c(t) - u(t)] dt = 0 \,.
\end{aligned} \tag{72}$$

Since the ROV must track straightlines or arcs of circumferences, the steady state value of the actual yaw rate is null or constant. Indicating the value above with $\bar{r}$, the result is:

$$\begin{aligned}
&m_u[\dot{u}_c(t) - \dot{u}(t)] \; + K m_u[u_c(t) - u(t)] + \\
&+ m_u[\bar{r}^2 \cos^2\psi_a(t)] \int_0^t \; [u_c(t) - u(t)] dt = 0 \,.
\end{aligned} \tag{73}$$

Dividing eq. (72) by m_u, gives:

$$\ddot{e}_u(t) \; + K\dot{e}_u(t) + [\bar{r}\cos\psi_a(t)]^2 e_u(t) = 0 \,, \tag{74}$$

where $e_u(t)$ is given by the first component of the vector (44). The eigenvalues given by the following equation:

$$\lambda^2 \; + K\lambda + [\bar{r}\cos\psi_a(t)]^2 = 0 \tag{75}$$

have to be real and negative, so the following constraint must be satisfied:

$$K > 2\bar{r}\sqrt{0.5\pi} \,. \tag{76}$$

If (76) is verified, then the solution of the equation (73) is a function which converges asymptotically to zero. Q.E.D. Now consider an ROV with two horizontal thrusters (see Fig. 2). This topology can be found in a real vehicle VideoRay ROV. The problem of the actuator allocation is a linear connection between the space of the vehicle's force and moment, i.e. $\tau_{uc}(t)$ and $\tau_{rc}(t)$, and the space of the actuator forces. Indicate the actuator control forces with $\tau_c^1(t)$ and $\tau_c^2(t)$. The result is:

$$\begin{bmatrix} \tau_c^1(t) \\ \tau_c^2(t) \end{bmatrix} = \begin{bmatrix} 1 & 1 \\ b & -b \end{bmatrix}^{-1} \begin{bmatrix} \tau_{uc}(t) \\ \tau_{rc}(t) \end{bmatrix} . \tag{77}$$

Remark 8. The errors (44) converge for all the values of the hydrodynamic masses.

Remark 9. Here, the fuzzy guidance control laws (47) have been converted into low level dynamic control laws (61). Therefore the low level control laws have been selected in

(60), so that the ROV exhibits the desired behaviour thus justifying the choice of the dynamic speeds given by (42). Also, by using the first three equations of the model (23), the dynamic speeds may be converted into actual position and orientation of the ROV. The measurement of the actual position and orientation using IMU can be affected by Gaussian noises due to the accelerometers and gyros. These noises cause non parametric uncertainties in the model of the ROV (cf. eq. 45). Therefore a KF in the feedback of the fuzzy control system has to be inserted, to merge the data provided by IMU and the exteroceptive sensors and obtain good estimates of the feedback signals.

3.4. KF in feedback of the Fuzzy control system for ROV localization

The discrete time KF deals with the case governed by the sampled stochastic odometric model given by (35). From output data provided by the IMU sensors, i.e. the accelerometer and the gyros, information about the actual positions and orientation feedback can be obtained. Since these information is corrupted by noises, a KF has to be introduced into the hierachical control system of the previous subsection. From the data provided by the GPS, USLB and IMU sensors, the KF estimates a filtered position and orientation signal for the feedback. The first equation of (35) gives the sampled state model to elaborate the data provided by the IMU sensors. Furthemore, the second equation of (35) gives GPS and USLB position and orientation measurements. Given the sampled model (35), we want estimates $\hat{\boldsymbol{\chi}}(k)$ of the state $\boldsymbol{\chi}(k)$ based on observation of the output $\boldsymbol{\xi}(k)$ alone. The task of the Kalman's filtering is to determine a set of Kalman gains $\mathbf{K}$ to minimize the variance of the estimation error, which is represented by $\mathbf{P}(k)$:

$$\mathbf{P}(k) = E\left\{ \left[\boldsymbol{\chi}(k) - \hat{\boldsymbol{\chi}}(k) \right] \left[\boldsymbol{\chi}(k) - \hat{\boldsymbol{\chi}}(k) \right]^{\mathbf{T}} \right\}. \tag{78}$$

Note that $\hat{\boldsymbol{\chi}}(k)$ is the feedback estimated state which is the output of the KF. Let us consider a state estimate $\overline{\boldsymbol{\chi}}(k)$ before measurement. The estimate $\overline{\boldsymbol{\chi}}(k)$ is found from $\hat{\boldsymbol{\chi}}(k-1)$ using the first equation of (35) with $\mathbf{w}(k\text{-}1)$=0. Thus it can be write:

$$\overline{\boldsymbol{\chi}}(k) = \mathbf{A}(k-1)\hat{\boldsymbol{\chi}}(k-1) + \mathbf{B}(k-1)\mathbf{u}(k-1) . \tag{79}$$

We also define the "*a priori*" error covariance:

$$\mathbf{N}(k) = E\left\{ \left[\boldsymbol{\chi}(k) - \overline{\boldsymbol{\chi}}(k) \right] \left[\left(\boldsymbol{\chi}(k) - \overline{\boldsymbol{\chi}}(k)\right) \right]^{\mathbf{T}} \right\} . \tag{80}$$

The function (80) is the solution of the following equation:

$$\mathbf{N}(k+1) = \mathbf{A}(k)\mathbf{P}(k)\mathbf{A}^{\mathbf{T}}(k) + \mathbf{R}_{\mathbf{w}} , \tag{81}$$

where $\mathbf{R}_{\mathbf{w}}$ is given by (31).
Now we seek the optimal gain:

$$\mathbf{K}_o(k) = \arg \min_{\mathbf{K}(k)} \operatorname{trace}(\mathbf{P}(k)) \tag{82}$$

Equation (82) minimizes the sum of the variance of the estimation errors given by:

$$\begin{aligned} &\operatorname{trace}(\mathbf{P}(k)) = \operatorname{var}\left[\left(x(k) - \hat{x}(k)\right)\right] + \\ &\operatorname{var}\left[\left(y(k) - \hat{y}(k)\right)\right] + \operatorname{var}\left[\left(\psi_l(k) - \hat{\psi}_l(k)\right)\right] \end{aligned} \tag{83}$$

Differentiating (83), it follows that:

$$\begin{aligned} &\frac{d \operatorname{trace}(\mathbf{P}(k))}{d\mathbf{K}(k)} = -2\left(\mathbf{C}(k)\mathbf{N}(k)\right)^{\mathbf{T}} + \\ &+2\mathbf{K}(k)\left(\mathbf{C}(k)\mathbf{N}(k)(\mathbf{C}(k))^{\mathbf{T}} + \mathbf{R}_{\boldsymbol{\rho}}\right) \end{aligned} \tag{84}$$

where $\mathbf{R}_{\boldsymbol{\rho}}$ is given by (32). Setting equation (84) to zero and solving for $\mathbf{K}(k)$ leads to:

$$\mathbf{K}_o(k) = \mathbf{N}(k)\mathbf{C}(k)\left(\mathbf{C}(k)\mathbf{N}(k)(\mathbf{C}(k))^{\mathbf{T}} + \mathbf{R}_{\boldsymbol{\rho}}\right)^{-1} \tag{85}$$

Calculating the function (78) in relation to the optimal gain given by (82), it follows that:

$$\mathbf{P}_o(k) = (\mathbf{I} - \mathbf{K}_o(k)\mathbf{C}(k))\mathbf{N}(k) \tag{86}$$

Based on the output observation, the following state is estimated:

$$\hat{\boldsymbol{\chi}}(k) = \overline{\boldsymbol{\chi}}(k) + \mathbf{K}_o(k)(\boldsymbol{\xi}(k) - \mathbf{C}(k)\overline{\boldsymbol{\chi}}(k)) \tag{87}$$

Let us summarize the discrete time recursive KF algorithm so far. The initial conditions $\overline{\boldsymbol{\chi}}(0)$ and $\mathbf{N}(0)$ have to be fixed. The steps are as follows:

1. evaluation of the optimal gain using the equation (85);
2. solving the equation of measurement update (87);
3. updating the error variance by using (86);
4. prediction of the future state using the equation (79);
5. prediction of the covariance error (cf. eq. 81)
6. updating the time and returning to step 1.

The KF gives $\hat{\boldsymbol{\chi}}(k)$ i.e. the estimated location of the ROV filtered by the noises. A digital to analogical converter (DAC) is able to obtain a time continuous variable $\hat{\boldsymbol{\chi}}(t)$, where a zero-order hold (ZOH) will produce a piecewise constant feedback state.

4. Experimental simulations

In this section simulation experiments are developed in a Matlab environment to show the performance of the proposed closed loop control system. The high level Fuzzy guidance control laws and the low level kinetic controller (cf. eqs. 47, 61) have been implemented. The KF algorithm has been implemented using C language with sequential acquisition and filtering of information provided by the IMU and the external sensors which have been simulated in a Matlab environment. Figs 9 and 10 show the block scheme of the hierarchical architecture proposed in this paper without and with KF. In case of hierarchical Fuzzy control without KF, the feedback signals are given by $x_n(t)$, $y_n(t)$ and $\psi_{\ln}(t)$ (cf. eqs. 27) (i.e. data provided by the IMU only), while in case of the same control strategy with KF, the feedback one is given

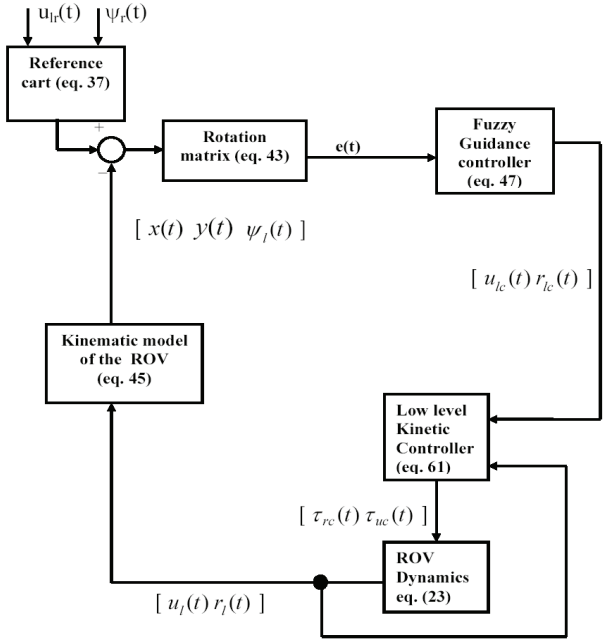

Fig. 9. Hierachical Fuzzy dynamic control system without KF.

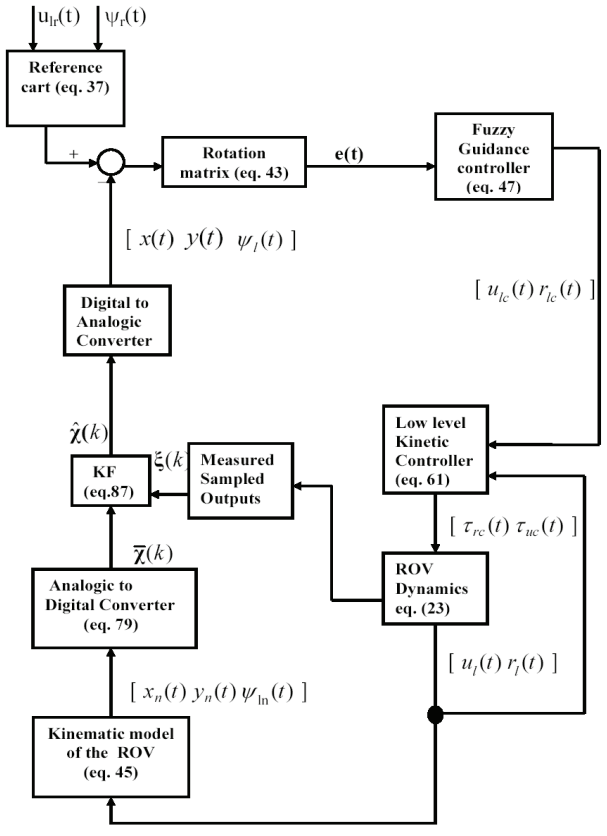

Fig. 10. Hierachical Fuzzy dynamic control system with KF.

by (87) (i.e. estimate of the filtered position of the ROV by using data of the IMU, GPS and USLB).

The simulation results are obtained using nominal parameters of a real ROV (Ridao P. et al., 2004), that is:

$$\begin{aligned} &m = 30kg, \\ &X_{\dot{u}} = Y_{\dot{v}} = 29.4462kg, \\ &N_{\dot{r}} = 1.5423kg \cdot m^2, \\ &I_z = 0.27kg \cdot m^2. \end{aligned} \tag{88}$$

The initial conditions of the KF are the following:

$$\begin{aligned} \mathbf{N}(0) &= \begin{bmatrix} 0.9 & 0 & 0 \\ 0 & 0.7 & 0 \\ 0 & 0 & 0.7 \end{bmatrix}, \\ \mathbf{R_w} &= \begin{bmatrix} 0.00005 & 0 & 0 \\ 0 & 0.00005 & 0 \\ 0 & 0 & 0.00005 \end{bmatrix}, \\ \mathbf{R_\rho} &= \begin{bmatrix} 0.2 & 0 & 0 \\ 0 & 0.2 & 0 \\ 0 & 0 & 0.2 \end{bmatrix}. \end{aligned} \tag{89}$$

The sample time of the discretization is:

$$T = 6 \cdot 10^{-4} s\,. \tag{90}$$

The numerical values of the fuzzy memberships are shown in Figs. 3 and 4.

Two simulation studies are developed. In the first simulation we compare the following cases:

1. hierarchical Fuzzy control with on-line KF (see Fig. 10);
2. hierarchical Fuzzy control without on-line KF (see Fig. 9).

Note that, if $f(\mathbf{e}(t)), g(\mathbf{e}(t))$ and $h(\mathbf{e}(t))$ are linear functions, then the properties given by (48)-(53) are verified. For this reason, second simulation compares the performances of the hierarchical control system in two cases:

- guidance laws (47) where $f(\mathbf{e}(t)), g(\mathbf{e}(t))$ and $h(\mathbf{e}(t))$ are obtained by using the fuzzy inference system with and without KF;
- guidance laws (47) where $f(\mathbf{e}(t)), g(\mathbf{e}(t))$ and $h(\mathbf{e}(t))$ are obtained as it follows :

$$\begin{aligned} f(e) &= k_1 abs(e_x), \\ g(e) &= k_2 abs(e_y), \\ h(e) &= k_3 abs(e_{\psi\, l}). \end{aligned} \tag{91}$$

with and without KF.

Case a) The following values are chosen for the reference speeds:

$$\begin{aligned} u_{rl}(t) &= 3m/s,\ \forall t, \\ r_{rl}(t) &= 3rad/s,\ \forall t. \end{aligned} \tag{92}$$

Fig. 11 shows the reference and the actual motion of the ROV by using the hierarchical control architectures shown in Fig. 9 and 10 respectively.

Remark 10. The circular trajectory of Fig. 11 does not violate the kinematic equations given by (37) and it is feasible when the ROV must inspect a limited area or an environment near the structure of interest.

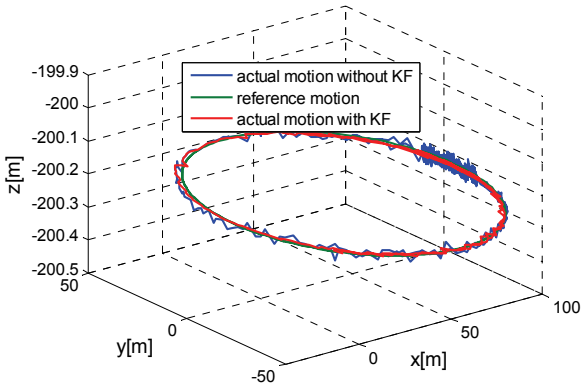

Fig. 11. Reference motion, actual motion of the ROV with and without KF

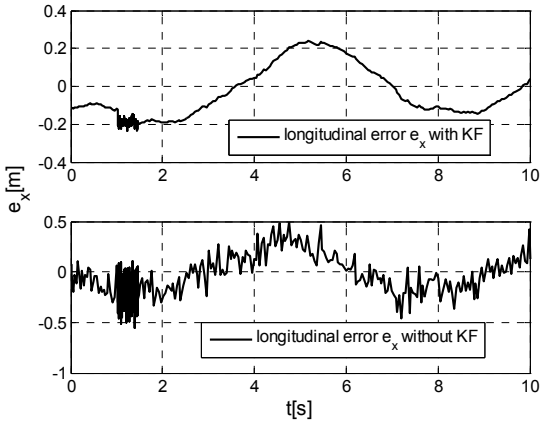

Fig. 12. Longitudinal motion error with and without KF.

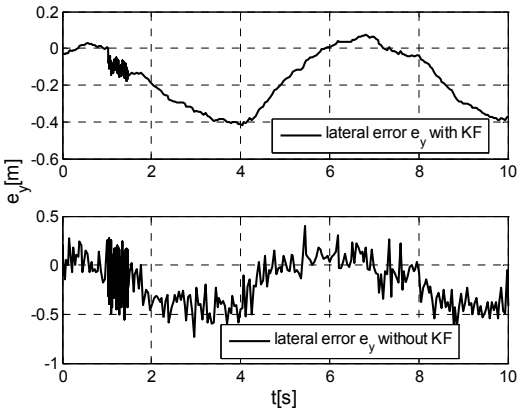

Fig. 13. Lateral motion error with and without KF.

Figs. 12 and 13 show the longitudinal motion errors in case of Fuzzy hierarchical control with and without KF.

Remark 11. Figs. 12 and 13 show that the motion errors are very small. It appears that the KF filters the measurements noises in a good way and improves the transient performance. It implies high accuracy in the horizontal motion control. Aleatory disturbances due to the marine environment have been introduced between 0 and 2s. Since they are not with Gaussian distribution, they are not filtered by the KF, but are compensated by the closed loop fuzzy control system.

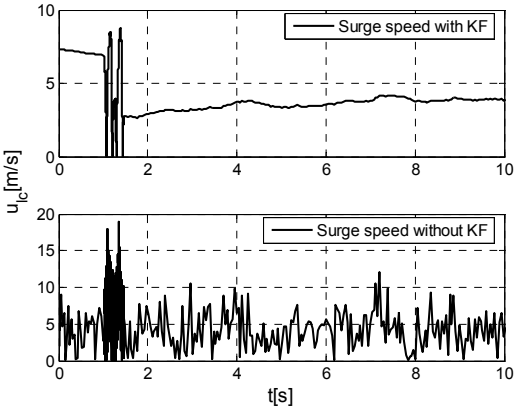

Fig. 14. Fuzzy linear speed control with and without KF.

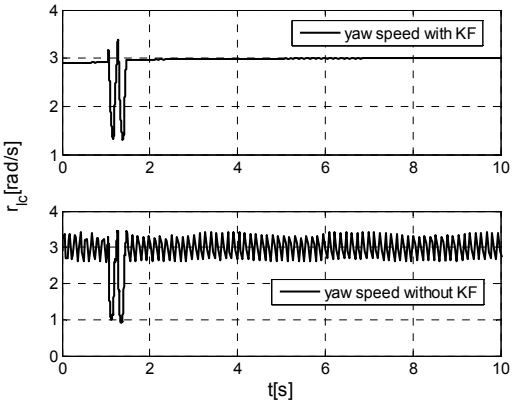

Fig. 15. Fuzzy yaw rate control with and without KF

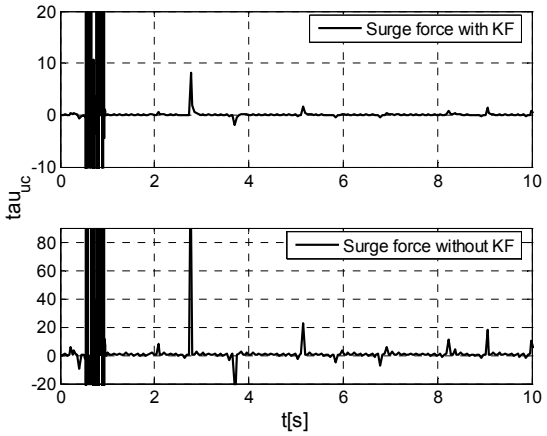

Fig. 16. Surge force control with and without KF

In figs. 14 and 15 the high level fuzzy guidance control laws are plotted with and without KF (cf. eqs. 47).

Remark 12. In Fig. 14 the linear control speed appears positive in all the times. Consequently (cf eqs. 21, 22), the surge speed control is a forward command. Also the on-line KF reduces the discontinuities of the signals above. Note that both the linear control velocity (cf. Fig. 14) and the yaw rate control (cf. Fig. 15) converge to the reference values given by (92).

Figs. 16 and 17 show the low level control signals with and without KF (cf. eqs. 61).

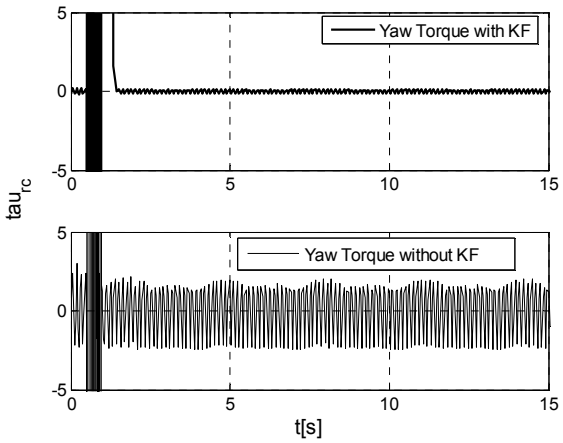

Fig. 17. Yaw torque control with and without KF

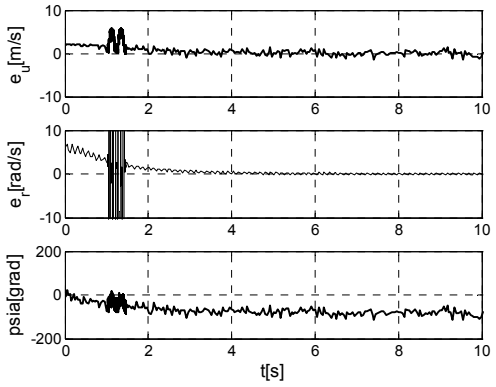

Fig. 18. Surge speed, yaw rate error and sideslip angle without KF

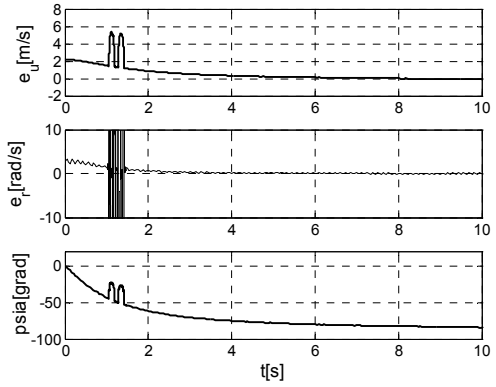

Fig. 19. Surge speed, yaw rate error and sideslip angle with KF

Remark 13. From Figs. 16 and 17 it is possible to observe the remarkable improvement obtained by using the on-line KF. In case of absence of KF, there are high frequencies of the surge force and torque control, because a random noise of the IMU is present which perturbs the dynamics of the fuzzy control system. By using the KF, the control system is able to offset this noise more easily than in case of absence and the high frequencies of the low level control signals are reduced. In other words, by merging Fuzzy control and KF, the control system is able to compensate the motion errors by lower torque and surge force values than in absence of KF.

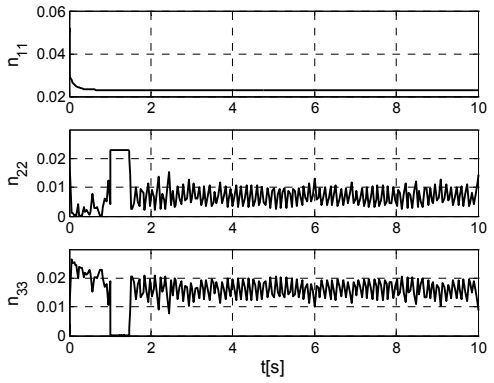

Fig. 20. KF errors covariances

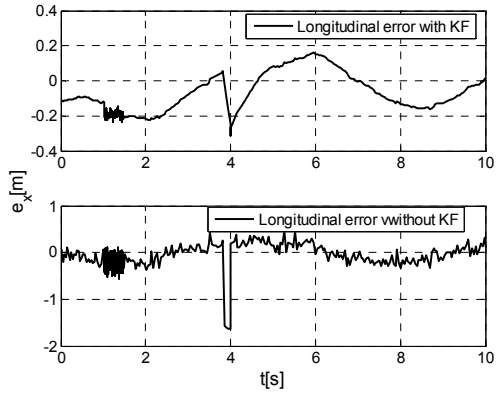

Fig. 21. Longitudinal motion error with perturbation

Figs. 18 and 19 show the speed errors (44) and the sideslip angle given by (20) with and without KF.

Remark 14. Figs. 18 and 19 show that the speed errors due to the application of the low level control laws plotted in Figs 16 and 17, converge to zero, as proved in Theorem 2. The sideslip angle is in the range given by (21). The on-line KF improves both the transient and the steady state.

Indicate with $n_{i\ i}(k)$ (i=1,2,3) the functions of the principal diagonal of the error covariance matrix given by (80). Figs. 20 shows the values of the covariance above in all the times.

Remark 15. The low covariance errors shown in Fig. 20 confirm the goodness of the feedback state estimation.

Now, consider outside disturbance violating the nominal motion of the ROV. Fig. 21 shows the performance of the fuzzy control systems with and without KF. The disturbance can be caused by impact of the ROV with the external marine environment. So the simulation tests consist of generating a step disturbance at the time 4s.

Remark 16. From fig. 21 it is evident that the KF filters the sensorial noises with good performances, but it does not filter the step disturbance. However the disturbance above is compensated by the closed loop fuzzy control both in case of presence of KF and in case of absence.

Case b) In this simulation experiment, results obtained by applying the high level control laws (47), where the functions $f(\mathbf{e}(t)), g(\mathbf{e}(t))$ and $h(\mathbf{e}(t))$ are obtained using the fuzzy inference mechanism and the analytical functions given by (91), are compared.

The initial conditions of the reference and ROV's positions and orientations are the following:

$$\begin{aligned} &x_r(0) = 0m, && x(0) = -30m \\ &y_r(0) = 0m, && y(0) = 20m \\ &\psi_{lr}(0) = 3.48rad && \psi_l(0) = 5.68rad \end{aligned} \tag{93}$$

In case of control law (47), where the functions are given by (91), it is:

$$k_1 = k_2 = k_3 = 5 \tag{94}$$

The planar reference trajectory and the actual horizontal motion of the ROV are shown in Fig. 22.

In Figs. 23 and 24 one considers the longitudinal and lateral motion errors for showing the transient state performances, in case of hierarchical control with Fuzzy inference (see Fig. 10) and in case of the same control system with functions given by (91).

Remark 17. Figs. 23 and 24 show the performance of the initial transient, where there is a lower response time of the motion errors in case of Fuzzy approach than in case of control system using the functions given by (91).

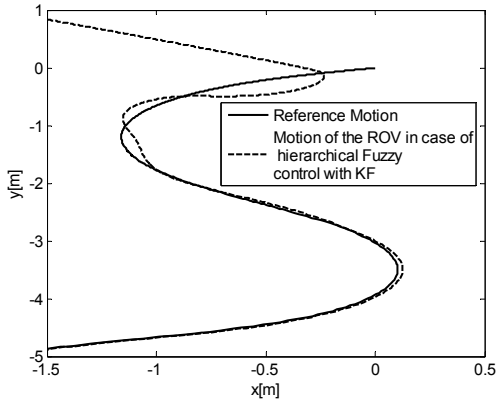

Fig. 22. Reference planar trajectory and ROV's actual motion using Fuzzy hierarchical architecture with KF

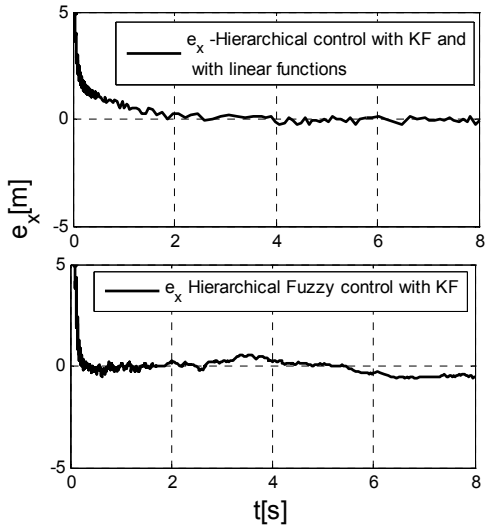

Fig. 23. Longitudinal error using functions given by (91) and fuzzy approach

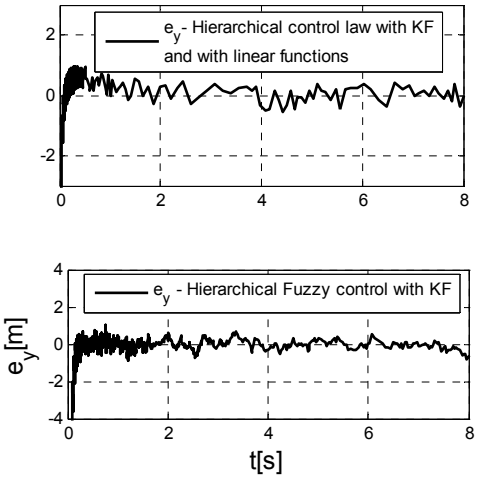

Fig. 24. Lateral error using functions given by (91) and fuzzy approach

5. Conclusions

In this paper a new Fuzzy/Kalman closed loop motion control system for underactutated ROVs has been developed. A merging of new high level fuzzy guidance commands, a new low level kinetic controller and an on-line KF has been presented. The fuzzy guidance commands ensure forward surge speed, saturation of the speeds control signals, robustness with respect to the perturbations due to the marine environment and lower response time of the motion errors than the hierarchical control without fuzzy. The asymptotical stability of the motion errors has been proved by using the Lyapunov's theorem and the properties of the fuzzy maps. The low level kinetic controller also ensures the convergence of the ROV's speeds to the fuzzy guidance commands. However the actual position and orientation of the ROV are corrupted by the sensorial noises of the IMU. Therefore a KF has been inserted in the feedback of the hierarchical fuzzy control. The KF filters the gaussian noises and improves the dynamical performance of the control system in terms of the motion errors and of the surge force and torque controls. Non-gaussian disturbances due to the marine environment and possible impacts of the ROV, can cause high values of the motion errors, but they have been compensated by the closed loop fuzzy control system with good transient and steady state performances, both in case of presence of KF and in absence.

6. Aknowledgement

All the Sections have been equally and jointly developed by the authors.

7. References

Akkizidis, I.S. ; Roberts G.N. ; Ridao P. & Batlle J. (2007). Designing a Fuzzy-like PD Controller for an

Underwater Robot. *Control Engineering Practice*, Elsevier, Vol. 11, pp. 471-480.

Antonelli, G. ; Fossen, T.I. & Yoerger, D.R. (2008). Underwater Robotics. In : *Springer Handbook of Robotics* (B. Siciliano and O. Khatib Eds), pp. 987-1008, Springer Verlag Berlin Heidelberg.

Caccia, M. (2007). Vision-based ROV Horizontal Motion Control : Near-seafloor Experimental Results. *Control Engineering Practice*, Elsevier, Vol. 15, pp. 703-714.

Caccia, M. & Verruggio, G. (2000). Guidance and Control of a Reconfigurable Unmanned Underwater Vehicle. *Control Engineering Practice*, Elsevier, Vol. 8, Issue 1, pp. 21-37.

Dai, J ; Zhao, X & Tan M. (2002). Fuzzy Logic Control in Autonomous ROV Navigation, *Proceedings of IEEE International Conference on TENCON 02*, pp. 1566-1569.

Dobref, V. & Tarabuta O. (2007). Thrust Optimization of an Underwater Vehicle's Propulsion System. *Annals of the Oradea University, Fascicle of Management and Tecnical Engineering*, Vol. 6, pp. 644-651.

Fabrizi, E. ; Oriolo G. ; Panzieri, S. & Ulivi, G. (1998). A KF Based Localization Algorithm for Nonholonomic Mobile Robots, *Proceedings of 6th IEEE Mediterranean Conference on Control and Systems,* pp. 130-135

Fossen, T.I. (1994). Guidance and Control of Oceanic Vehicles. New York, Weeley.

Hagen, P.E. ; Hegrenaes, O. ; Jalving, B. ; Midtgaard, O. ; Wiig, M. & Hagen, O. K. (2009). Making AUVs Truly Autonomous. In *Underwater Vehicles* (Alexsander V. Inzartsev Ed), pp. 129-152, In-tech.

Jalving, B. ; Gade, K. ; Hagen, O.K. & Vestgard, K. (2003). A Toolbox of Aiding Techniques for the Hugin AUV Integrated Inertial Navigation System, *Proceedings of IEEE International Conference on Oceans 2003 MTS/IEEE.*

Jwo D.J. ; Chen M.Y. ; Tseng C.H. & Cho T.S. (2009). Adaptive and Nonlinear Kalman Filtering for GPS Navigation Processing. In *Kalman Filter : Recent Advances and Applications* (Victor M. Moreno and Alberto Pigazo Eds.), pp. 321-347, In-tech.

Koh, T. ; Lau, M.W.S. ; Low, E. ; Seet, G. ; Swey, S. & Cheng P. (2002). Development and Improvement of an Underactuated Robotic Vehicle, *Proceedings of IEEE Conference on Oceans 2002*, Vol. 4, pp. 2039-2044.

Miskovic, N. ; Vukic, Z. & Barisic, M. (2009). Identification of Underwater Vehicles for the Purpose of Autopilot Tuning. In *Underwater Vehicles* (Alexsander V. Inzartsev Ed), pp. 327-347, In-tech.

Ontini, M. (1998). ROVs : Analysis and Evolution of the Market. *Underwater Magazine*.

Raimondi, F.M. & Melluso, M. (2008). Trajectory Decentralized Fuzzy Control of Multiple UAVs, *Proceedings of IEEE International Conference on Advanced Motion Control*, pp. 455-461, Trento (Italy).

Raimondi, F.M. & Melluso, M. (2007). Fuzzy Adaptive EKF Motion Control for Non-holonomic and Underactuated Cars with Parametric and Non parametric Uncertainties. *IET Control Theory and Applications*, Vol. 1, Issue 5, pp. 1311-1321.

Ridao P.; Batlle E. ; Ribas D. & Carreras M. (2004). Neptune :a HIL Simulator for Multiple UUVs, *Proceedings of IEEE International Conference on Oceans 04*, pp. 524-531.

Valavanis K.P. ; Gracanin D. ; Matijasevic, M. ; Kolluru, R. & Demetriou, G.A. (1997). Control Architectures for Autonomous Underwater Vehicles. *IEEE Control Systems Magazine*, Vol. 17, Issue 6, pp. 48-64.

Yoerger, D.R. & Slotine J.E. (1991). Adaptive Sliding Control of Underwater Vehicles, *Proceedings of IEEE International Conference on Robotics and Automation*, pp. 2746-2751.

Yoerger, D.R. & Slotine J.E. (1985). Robust Trajectory Control of Underwater Vehicles. *IEEE Transactions on Oceanic Engineering*, Vol. 10, Issue 4, pp. 462-470.